Long-term Variation of Dust Devils in East Asia during 1959-2021

P. Du[1], Z. Huang[1, 2*], S. Tang[1], Q. Dong[1], J. Bi[1], X. Yu[1], Q. Gu[1]

[1]Collaborative Innovation Center for Western Ecological Safety, College of Atmospheric Sciences, Lanzhou University, Lanzhou, China.

[2]Collaborative Innovation Center on Forecast and Evaluation of Meteorological Disasters (CIC- FEMD), Nanjing University of Information Science & Technology, Nanjing, China.

Corresponding author: Zhongwei Huang (huangzhongwei@lzu.edu.cn)

Key Points:

- An overall downward trend in dust devil frequency in East Asia during 1959-2021 where the strong ones dropped significantly at the fastest rate.
- Dust devils in the Taklimakan Desert decreased while they increased significantly in the Gobi Desert.
- There is a negative correlation between precipitation and dust devil frequency.

Abstract

Dust devils play an important role in dust transport by carrying it from surface into the atmosphere, especially in summer. However, information on how dust devil changed in the past decades and what caused these changes remains lacking. Based on thermodynamic criterion and ERA5 reanalysis dataset, this study investigated long-term variation of dust devil in East Asia over the past 60 years. We found the annual mean frequency of dust devil in East Asia was approximately 8.2×10^5 hours for 1959 to 2021. In particular, it is shown that an overall downward trend in dust devil frequency over the study period in East Asia, among which strong dust devils declined significantly at the fastest rate while the weak ones dropped insignificantly. Moreover, dust devil frequency in the Gobi Desert (GD) increased obviously but they decreased in the Taklimakan Desert (TD). It is represented that there was a peak for monthly variation of dust devil, shifting from June to July, over the past decades. For the diurnal changes, dust devils mainly occurred between 10:00 and 16:00 at Local Time (LT), with over 60% of them happening between 12:00 LT and 14:00 LT. We also found a negative correlation between precipitation and dust devil frequency. This study provides a comprehensive understanding of dust devils in East Asia over the past decades, which is of great importance to further evaluate its impact on climate, environment as well as ecosystem.

1 Introduction

Dust devils are convective vertical vortices caused by uneven surface heating, commonly happening in arid and semi-arid regions (Klose et al., 2016). The occurrence of dust devils requires certain meteorological conditions such as local vorticity and strong frequent isolation which can lead to atmospheric vertical

instability with super adiabatic lapse rate (Balme and Greeley, 2006). Flat terrain with dust sources is also a prerequisite for the presence of dust devils. It is shown that arid areas are the most susceptible to dust devils (Balme and Greeley, 2006). In the presence of dust devil, earlier measurements have shown that the dust concentration in the atmosphere is three orders of magnitude higher than background value. A typical dust devil can bring approximately 20 kg of dust into the atmosphere, while a very large one with radius of over 100 m can carry about 15, 000 kg of dust during its life span (Koch and Renno, 2005; Renno et al., 2004).

The mineral dust that has been lifted in the air can directly and indirectly affect climate which can in turn alter radiation balance in the atmosphere and act as cloud condensation nuclei (CCN) to influence precipitation (Ginoux et al., 2001; Huang et al., 2010; Zhang et al., 2022). Direct effect of dust aerosols on radiation balance (through absorption and scattering) influences the energy balance of earth system (E-cycle), while the organic matters carried by dust is associated with the carbon cycle (C-cycle) (Dong et al., 2022; Huang et al., 2022; Liu et al., 2022; Shao et al., 2011). Besides, the absorption of solar radiation by dust aerosols can also change the relative humidity and stability of the atmosphere (considered as semi-direct effect) and thus modifies cloud properties, such as cloud lifetime and cloud liquid water content (Huang et al., 2014; Huang et al., 2018). It is indicated that the frequency of dust devils will increase as surface cover decreases (Oke et al., 2007). In the context of global warming, drylands which feed about 38% of the world's population are more sensitive and vulnerable to the risk of drought area expansion and intensification that may increase the frequency of dust devils (Huang et al., 2017). Therefore, it is essential to investigate the spatial and temporal distributions of dust devils, and its inter-annual variability and effects.

Field observations have been conducted to investigate the properties of dust devils in the past decades. These studies revealed that the size and duration of a typical dust devil is about tens to over 100 meters and lasts for about 5-15 minutes which usually occurs between 10:00 am and 17:30 pm local time (Carroll and Ryan, 1970; Sinclair, 1973; Hess and Spillane, 1990; Balme and Greeley, 2006). Dust devil occurrence requires the temperature difference between surface and air of more than 15 ℃, perhaps more specifically, above 17 ℃ and the favorable wind speeds are about 2-7 $m \cdot s^{-1}$ (Ansmann et al., 2009; Liu et al., 2016; Oke et al., 2007). Large eddy simulation (LES) has been used as an effective method to study dust devils. Pressure drop is an important indicator about the intensity of dust devils in the LES method because more intense pressure drops can bring more dust loadings and it is relatively easy to measure (Gu et al., 2008; Klose and Shao, 2016). Nonetheless, if there is not enough loose material on the surface to be carried into the atmosphere, the loading of dust devil will not increase with more intense pressure drop (Mason et al., 2014; Klose et al., 2016). Based on the LES method, Gu et al. (2010) demonstrated the strong impact of initial angular momentum of air parcels on the radius of dust devils and significant influence of surface heat flux on updraft velocity.

Using the similar method, some studies also showed that particles up to 160 m in diameter could be rolled into the atmosphere with large ones dropping back to the ground while small ones were lifted to a certain height and transported elsewhere (Zhao et al., 2004; Gu et al., 2008). Recently, there have been some attempts to evaluate the contribution of dust emissions by dust devils. By combining observation data and theory, Koch and Renno (2005) found that the contribution of dust devils to total global dust emissions was up to 35%. By applying thermodynamic criteria, Jemmett-smith et al. (2015) presented the global hourly potential dust devil occurrence, and estimated the amount of dust from dust devils as approximately 3.4% of the global total. Besides, other studies focused on arid region in the northwestern China, mainly around the Taklimakan Desert. Han et al. (2016) estimated that dust devils contributed 53% to total annual desert dust in the western China based on satellite and Lidar observations. By combining observed meteorological data and estimation model, Ma et al. (2020) gave an estimate of 46.5% for the same region. Therefore, there is still large uncertainty about the impacts due to the complexity of dust devils and the lack of knowledge of their characteristics in different regions.

Whilst previous studies presented a general idea of the properties of dust devils and the amount of dust they could bring, they did not dip into the spatial-temporal change and give a long-term trend. In addition, East Asia is an important dust source region that contributes about 11 % of global dust loading (2.0–3.4 Tg) (Kok et al., 2021). Combined with its geographical location and meteorological conditions, East Asia is a favorable area for dust devils (Jemmett-smith et al., 2015). Nevertheless, there are limited studies that focus on dust devils in East Asia and distinguish the impact of different underlying surfaces. Until now, information on how dust devil changed in the past decades and what caused these changes is still lacking. This manuscript describes our comprehensive investigation on dust devils in East Asia. Section 2 gives a description of date and methods. The overall distribution and trend of dust devils in East Asia as well as a detailed discussion in four selected sites with different underlying surface and meteorological conditions are presented in section 3. Conclusions are given in section 4.

2 Data and Methods

2.1 Study area

Fig. 1 presents the four selected region in East Asia for detailed investigation. We chose the region within the range of 70°-140°E and 15°-55°N for our study. The selection of four regions is based on the annual average frequency of dust devils and takes dust source into account. TD, TK, TB and GD in Fig. 1 represent the Taklimakan Desert, Turpan Basin and Kuluketage, Tsaidam Basin and Gobi Desert, respectively. The four regions are all located in arid areas with sufficient sand supply. Each region has the same latitude and longitude scale spanning 6.25 longitudes and 3 latitudes (see details in Table 1). Annual mean precipitation was obtained from ERA5 (the fifth generation ECMWF atmospheric reanalysis of the global climate) reanalysis dataset, we use the

average of 1959-2021 in this study (more details in section 2.3). Following the Food and Agriculture Organization of the United Nations (FAO), the arid index (AI) is defined as the ratio of the annual precipitation (P) to the annual potential evapotranspiration (PET) and calculated by applying the Climate Prediction Center (CPC) datasets (FAO, 1977; Feng and Fu, 2013; Huang et al. 2020). Combined with Feng and Fu (2013), aridity of a region can be classified as dryland (P/PET<0.5), hyper-arid (P/PET $<$ 0.05) and arid (0.05 $<$ P/PET $<$ 0.2). AI in Table 1 is the average for 2011 -2016 and all four regions listed are located in arid region with AI<0.2 while TB and TK are further in the hyper-arid region. Annual mean dust devil frequency in Table 1 is calculated using the thermodynamic criteria in section 2.2 and ERA5 reanalysis dataset.

Table 1. Basic information of the four regions in this study.

Location	Longitude and Latitude range	Underlying surface type	Annual mean precipitation (mm)	Arid Index (AI)	Annual mean dust devil frequency ($\times 10^4$Hours)
Taklimakan Desert (TD)	°E-87.25°E, 38°N-41°N	Desert	±14.2		±0.91
Turpan Basin and Kuluketage (TK)	°E-94.25°E, 40.5°N-43.5°N	Basin	±19.2		±0.98
Tsaidam Basin (TB)	°E-97.25°E, 36.25°N-39.25°N	Basin	±23.8		±1.33
Gobi Desert (GD)	°E-106.75°E, 41.5°N-44.5°N	Desert	±25.6		±0.65

2.2 Identification of dust devils

Basically, the thermodynamic criteria used in the study are from Jemmett-smith et al. (2015) who summarized previous studies and verified them. The criteria include $w^*/u^* > 5.0$ (Lyons et al., 2008) and 8.5 K m^{-1} near-surface lapse rate (Ansmann et al., 2009). High near-surface lapse rate implies strong surface heating due to solar irradiation while $w^*/u^* > 5.0$ constrains the boundary layer conditions. The 8.5 K m^{-1} near-surface lapse rate criterion was derived from observations in North Africa (Ansmann et al., 2009) which is consistent with

that in the Taklimakan Desert (Liu et al., 2016). In the $w^*/u^* > 5.0$ criterion, u^* and w^* represent the frictional dissipation and convective buoyancy, respectively. According to Deardorff [1970], w^* can be calculated using

$$w_* = \left[\frac{g}{\overline{T}} h(\overline{\mathrm{T}})_0\right]^{\frac{1}{3}} \quad (1)$$

where $\frac{g}{\overline{T}}$ is the buoyancy parameter for an ideal gas, h is the height of boundary layer, and $(\overline{\omega T})_0$ is the kinematic heat flux near the surface. By applying the thermodynamic criteria, Jemmett-smith et al. (2015) gave the global hourly climatology of potential dust devil and dusty plume (PDDP) occurrence which is consistent with observations with appropriate daily and seasonal changes. Based on the same criteria, we comprehensively investigate the distribution of dust devils in East Asia and the factors influencing them.

2.3 ERA5 reanalysis dataset

Assessed by Hersbach et al. (2021), ERA5 is the fifth-generation climate reanalysis dataset from ECMWF (the European Centre for Medium-Range Weather Forecasts) produced by the Copernicus Climate Change Service (C3S, 2017). Briefly, ERA5 was developed to replace its predecessor ERA-Interim (Dee et al., 2011) with finer spatial grid (0.25°×0.25°), higher time resolution (hourly) and more vertical levels currently available from 1959 to present. It was constructed using 12-hourly 4DVar data assimilation model combined with vast amounts of data (e.g., model forecast, data from historical satellite, in-situ observations, etc). The ERA5 outputs used in this paper are hourly grid points of temperature, surface pressure, friction velocity, boundary layer height, surface sensible heat flux, total precipitation and wind. Near-surface lapse rate in the thermodynamic criteria is calculated using surface and 2 m air temperature while w* is calculated using Equation (1) in which the value of surface sensible heat is $(\overline{\omega T})_0$ and T can be approximated to 925 hPa potential temperature using Equation (2),

$$\theta = T\left(\frac{P_{00}}{P}\right)^{K} = T\left(\frac{P_{00}}{P}\right)^{\frac{R}{C_P}} \quad (2)$$

where T is the surface air temperature, P is the surface pressure, P_{00} is the 925 hPa. By using the outputs and equations listed above, we can employ the criteria to calculate dust devil frequency.

3 Results and Discussion

3.1 Variation of Dust Devils in East Asia

According to the thermodynamic criteria (refer to section 2.2), the calculated annual mean dust devil frequency during 1959-2021 is shown in Figure 1. The shade of color represents dust devil frequency, where the darker the color, the higher dust devil frequency. Arid area is indicated by grey dots. The highest frequency of annual average dust devil occurred in the northwestern Tibet with

more than 1000 hours which occupy 11% of the yearly time. In contrast, dust devils are rare at middle and high latitudes and in humid regions. For regions at middle and high latitudes, the reason is insufficient intense surface heating through insolation. Therefore, the near-surface atmospheric temperature lapse rate is not strong enough to generate dust devils. For humid regions, rainfall can restrain the occurrence of dust devils by altering soil moisture (Liu et al., 2016; Klose et al., 2016). The areas with high frequency of dust devils, i.e., the dark-colored areas in Figure 1, largely overlap with the drought-prone areas dotted in gray. This implies that arid and semi-arid regions with dust source are the areas with frequent occurrence of dust devils, consistent with previous studies, except for the Qinghai-Tibet Plateau (Jemmett-smith et al., 2015; Klose et al, 2016). The Tibetan Plateau is not in the northwest arid zone but has a high frequency of dust cyclones, which can be attributed to the long hours of sunshine, thin air as well as its sparse vegetation cover. Strong solar radiation due to its high altitude in the Qinghai-Tibet Plateau with average solar radiation reaching 6400 MJ/ ($m^2 \cdot$ year) and highest values in its northwest region is another favorable condition for dust devils (Balme and Greeley, 2006; Liu et al., 2022). All those factors together make it reasonable for the high frequency of dust devils to occur in the Qinghai-Tibet Plateau. The frequency of dust devils within the red box that we selected has an average annual hour ranging from 10^4 to 10^5 which takes up 1.5% to 5% of the yearly time. Due to the complex topography of the Tibetan Plateau and the lack of observational data, a small area on the Tibetan Plateau, though having high dust devil frequency, was not selected in this study. The dust devil on the Qinghai-Tibet Plateau is worth studying and this part of the gap can be filled by future observations.

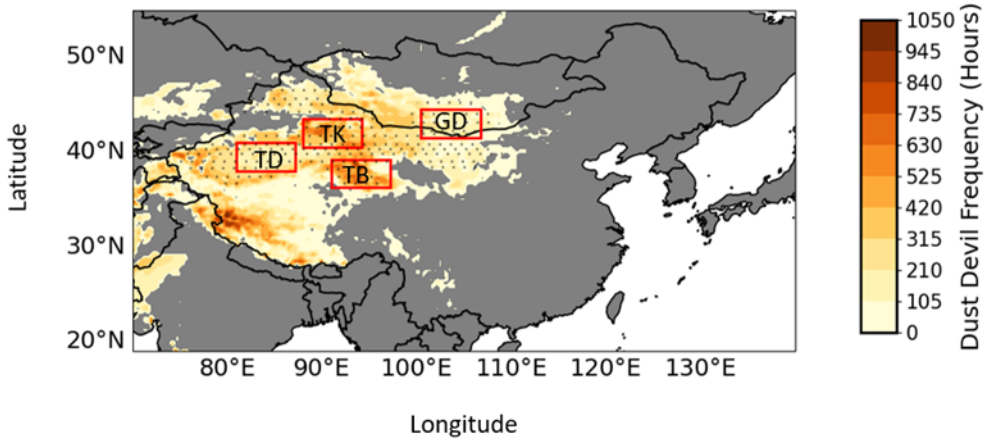

Figure 1. Distribution of dust devil frequency during 1959-2021 calculated using ERA5 reanalysis dataset. Four study regions are marked by red box, grey

dots represent typical dust sources in East Asia.

Previous studies have demonstrated that near-surface lapse rate which represents the development of an unstable lower atmosphere is critical for the occurrence of dust devils. As the lapse rate increases, dust devils tend to have larger diameters (Oke et al., 2007; Ryan et al., 1972). Therefore, we use near-surface lapse rate to determine the intensity of dust devils. Near-surface lapse rate at the duration of dust devils from 1959 to 2021 was calculated (see Figure 2). It has a normal distribution with a mean of 8.5, and a standard deviation of 1.5. Based on the graph, we give the criteria for classifying different intensities of dust devil. Dust devil is considered strong when it is greater than two standard deviations, that is, when the near-surface lapse rate is greater than 11.5°C; medium when it is between one standard deviation and two standard deviations; weak when it is within one standard deviation, that is, near-surface lapse rate is less than 10°C. All strengths of dust devils satisfy the criteria of $w^*/u^*>5$. By this definition, the frequency of weak dust devils is approximately 68% of the total frequency of occurrence while the strong ones account for less than 5% of the total frequency. Since the criterion for occurrence of dust devils is given as 8.5 K near-surface lapse rate, we give the horizontal coordinates of Figure 2 starting from 8.5.

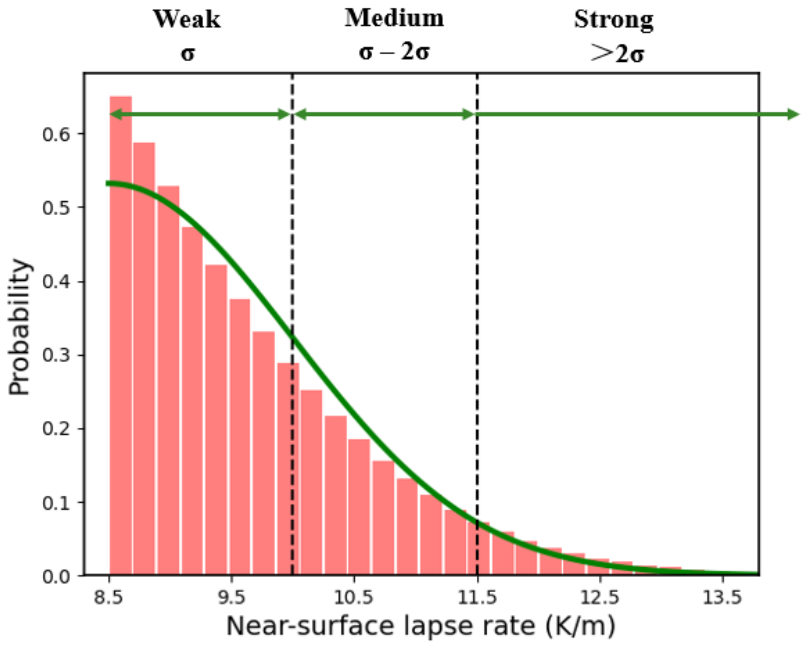

Figure 2. Frequency distribution of near-surface lapse rate calculated using ERA5 reanalysis dataset.

According to the criteria discussed earlier, the variation of dust devils of different

intensities from 1959 to 2021 based on ERA5 is displayed in Figure 3. Due to the complex topography of the Qinghai-Tibet Plateau region, the occurrence of dust devils and the criteria for their occurrence need to be further verified. Thus, only the arid regions of the northwestern China and the Gobi Desert were selected for the calculations in Figure 3. The annual mean potential dust devil frequency from 1959 to 2021 in East Asia was approximately 8.2×10^5 hours, of which the frequency of weak dust devils was about 5.8×10^5 hours, the frequency of medium ones was roughly 2.1 $\times10^5$ hours, and the frequency of strong dust devils was about 3.8×10^4 hours. The trend of dust devils varied with different intensities. There is a clear downward trend of strong dust devil, while weak dust devil had a great inter-annual fluctuation during 1959-2021, but the trend line of occurrence frequency was basically horizontal in general, and the trend of moderate intensity dust devil was somewhere in between. In Figure 3, all four lines experienced a significant drop in 1992-1993, which could be the effect of the eruption of Mount Pinatubo in June 1991 that caused a global surface cooling of about 0.4 ℃ in the following two years (Self et al., 1996). The frequency of dust devils gradually picked up after the eruption with weak dust devils rising to a level of the 1960s. Gillette et al. (1990) distinguished the different sizes of dust devils and gave the estimated dust flux per dust devil, where the flux of a small dust devil with size was 2.2 g cm^{-2} s^{-1}, a moderate dust devil was 20.9 g cm^{-2} s^{-1}, and a large dust devil was over 200 g cm^{-2} s^{-1}. The results from Gillette et al. (1990) implied that strong dust devils could be several orders of magnitude greater than weak dust devils in terms of dust flux which is consistent with other studies (Metzger et al., 2011; Neakrase et al., 2010). Although the amount of dust brought in each time was small, weak dust devils occurred more frequently than strong dust devils, and could be regarded as a more significant vehicle for dust to enter the atmosphere from the ground than strong ones.

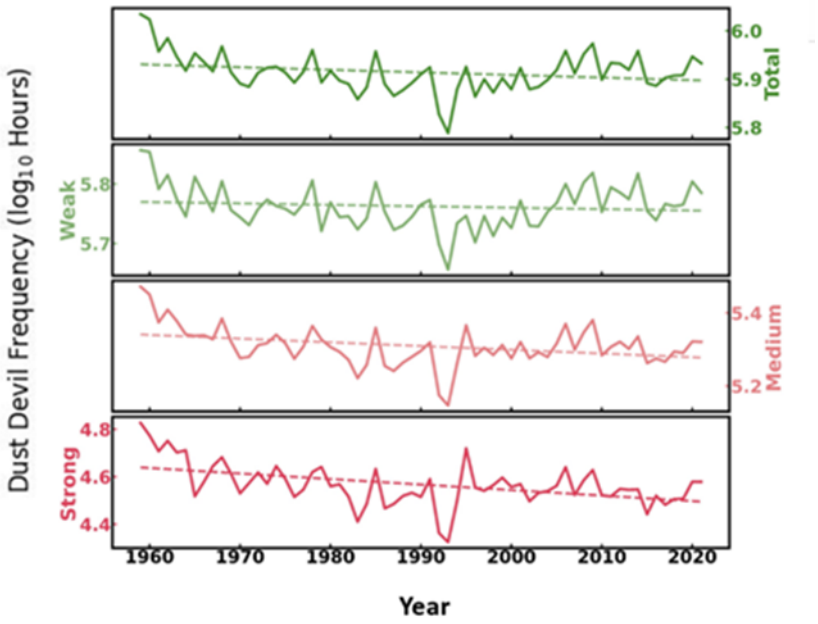

Figure 3. Yearly change of dust devils for different intensities calculated using ERA5 reanalysis dataset.

Figure 4 shows the seasonal mean distribution of dust devil in East Asia during 1959-2021 based on ERA5. Similar to Figure 1, darker color represents higher dust devil frequency. The highest frequency of dust devils occurred in summer which was 5.3×10^5 hours, followed by spring (2.5×10^5 hours) and autumn (4.4×10^4 hours), and almost no dust devils occurred in winter. In summer, the areas with high frequency of dust devils largely coincide with drought areas which have rich sources of dust. Southwest side of the Qinghai-Tibet Plateau, Tsaidam Basin and the edge of Taklimakan Desert showed high value areas for the occurrence of dust devils. Since dust storms usually occurred in spring and winter but rarely in summer, dust devils become a major means of transporting dust aerosols into the atmosphere in summer which could further impact on weather and climate with aerosol–radiation and aerosol–cloud interactions (Gao et al., 2021). In addition, the dust that has been lifted in the atmosphere could function as a carrier of bioaerosols which are efficient ice nuclei (IN) and cause adverse health effects, e.g., allergies, toxic effects, and infectious diseases (Després et al., 2012). Occurrence of dust devils requires frequent strong insolation as well as anomalously high soil temperatures, making it reasonable for them to occur most frequently in summer (Balme and Greeley, 2006). Those results are also consistent with previous studies. Han et al. (2016) indicated that dust devils reached the highest value in summer while Gillette and Sinclair (1990) reported about the seasonality of dust devil with the maximum in summer and the minimum in winter. Based on LES method, Klose (2014) estimated the number of dust devils and found the largest number of dust devils in spring and

summer. More detailed analyses of the monthly and decadal changes are given in the following paragraphs. Wang et al. (2021) found that summer length in the Northern Hemisphere midlatitudes extended from 1951 to 2011 and would continue to lengthen in the 21st century. The extended summer might cause more dust devils which would bring more dust into the atmosphere.

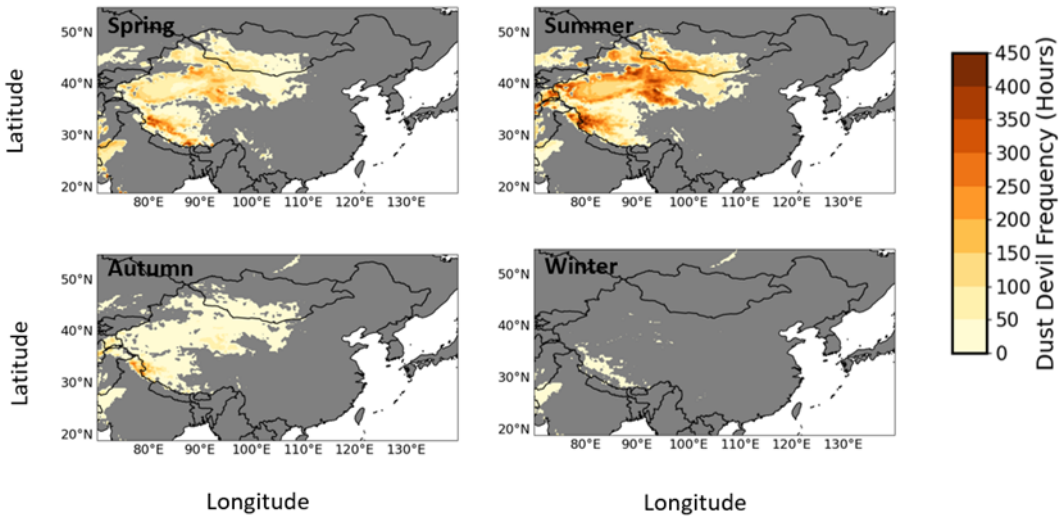

Figure 4. Seasonal mean distribution of dust devil in East Asia during 1979-2021 calculated using ERA5 reanalysis dataset.

Besides the distinct seasonal variation, the monthly change in the frequency of dust devils is also evident. Figure 5 shows the monthly variation of dust devils in East Asia for different decades. The thick solid line in the middle is the average occurrence of dust devils for each month of the decade, while the shaded areas next to it are one standard deviation above and one standard deviation below the average, respectively. In these six decades, the annual change in the frequency of dust devils is single-peaked. The frequency of dust devils began to rise from March onwards, reaching a peak in June and July, then gradually declining, and after September the dust devil basically did not occur. The standard deviation of the frequency of dust devils from May to August was large, while the standard deviation of the other months was small, which indicates that the frequency of dust devils varied greatly from May to August during the decade, while the frequency was relatively stable in other months. The large standard deviation from May to August also suggests that for the same region, the effect of different meteorological conditions in different years on the frequency of dust devils is mainly concentrated in May-August, with little effect on dust devils in other months. Comparing the six subplots, there is a tendency for the peak to move from June to July. Dust devil occurrence peaked in June in the 1960s, and it peaked in July in the 2010s with relatively small

standard deviation. For the other decades, the maximum value of dust devil frequency fluctuated back and forth between June and July with large standard deviation. The largest standard deviation occurred in the 1990s, when the effect of the Pinatubo eruption caused greater inter-annual fluctuations in the dust devils. By comparing the height of the peaks in different subplots, it is found that the frequency of dust devils is high in the 1960s, low in the 1970s, 1980s, 1990s, and then increased in the 2000s and 2010s, which is consistent with the results in Figure 3. Han et al. (2016) gave the similar distribution of dust devil frequency as well as monthly dust emissions by dust devils in his study and found that without the effect of dust storms, the optical thickness monthly variation was consistent with monthly changes in dust devil thermodynamic efficiency which reflects the dust devil strength. Lyons et al. (2008) also found the single peaked distribution of dust devil annual variation in Australia. However, there are few studies on the tendency of peak movement. Based on the available data, we can preliminarily make this assumption and see how the dust devil would develop in the future.

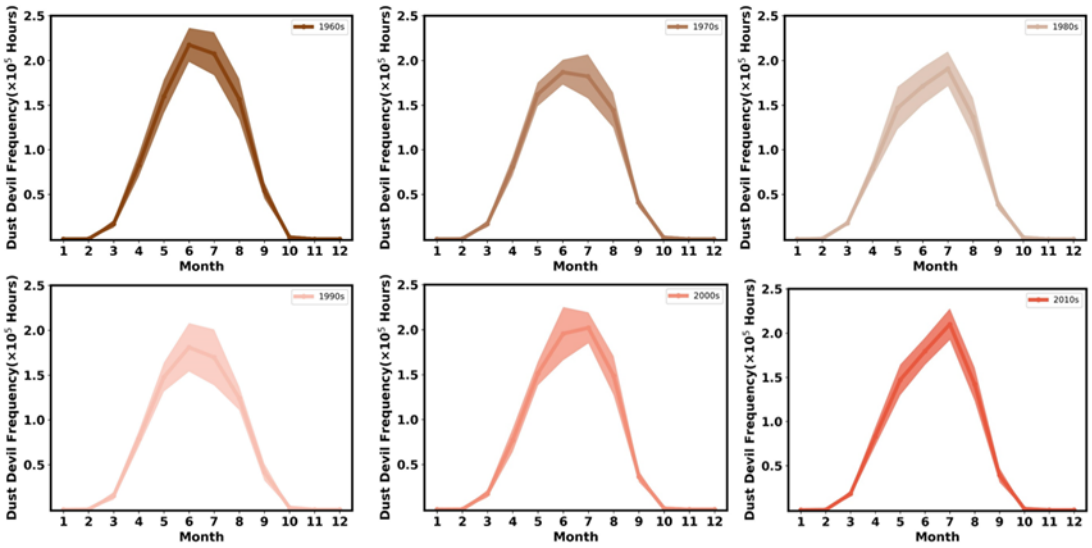

Figure 5. Monthly variation of dust devils in East Asia over the past decades calculated using ERA5 reanalysis dataset.

3.2 Variation of Dust devils at four specific regions

Due to the different underlying surface and meteorological conditions in different parts of East Asia, the characteristics of dust devils can vary considerably. Here we describe the dust devils in small areas.

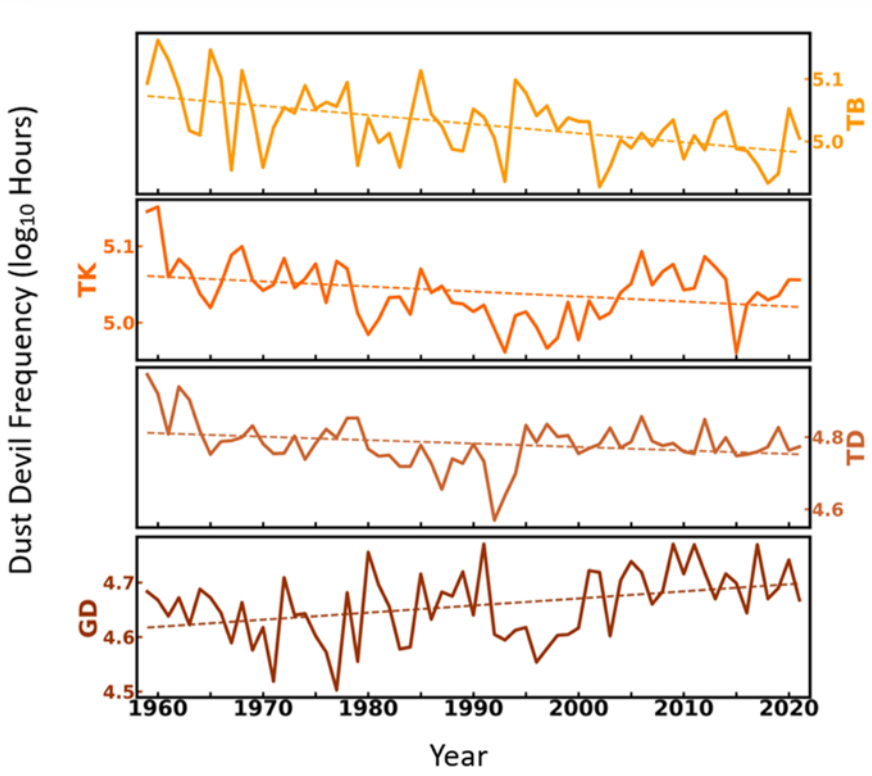

Figure 6. Long-term variation of dust devil for four sites during 1959-2021.

The annual variation of dust devils in four selected regions is shown in Figure 6. TD, TK, TB and GD represent the Taklimakan Desert, Turpan Basin and Kuluketage, Tsaidam Basin and Gobi Desert, respectively (see detailed description in section 2.1). These four regions have different trends in dust devil frequency during 1959-2021, with a decreasing trend for TK, TB, and TD, and an increasing trend for GD. The tendency for TB, TK, GD satisfied $p < 0.01$, passing the 0.01 statistical test criterion; while TD passed the 0.05 statistical test criterion. The different tendency indicates the different variability of dust devil frequency in different parts of the same region. Therefore, in future research, in order to have an accurate understanding of dust devil variability, it would be interesting to study not only large scale dust devils, but also small area variability. Similar to Figure 3, there was an obvious decline in dust devil frequency during 1992-1993, but the impact of the Pinatubo eruption was distinct for different regions. In the Gobi Desert, insolation is the main constraint due to its relatively high latitude whereas the other three areas have adequate solar radiation for dust devils to occur. Due to the eruption of Mount Pinatubo in 1991, the net radiation arriving at the Earth's surface has decreased dramatically (Self et al., 1996). Therefore, reduction in the net radiation caused by the Pinatubo eruption has mainly affected the frequency of dust devils in the TD, TK and TB, making

the previously favorable insolation conditions no longer sufficient. Variation of dust devil frequency from the mean over different decades is shown in Table 2. Each number in the table is the growth rate with respect to the 63-year average dust devil frequency in the corresponding area. For the GD and TB, the trend in dust devil frequency variation over the 63-year period was uniform, while for the TK and TD, dust devil exhibited a tendency to decrease and then increase, with low values in the 1980s and 1990s, followed by an increase in dust devil frequency in the 2000s and 2010s. The different tendencies in four regions rely on the variation of their local meteorology (details in section 3.3).

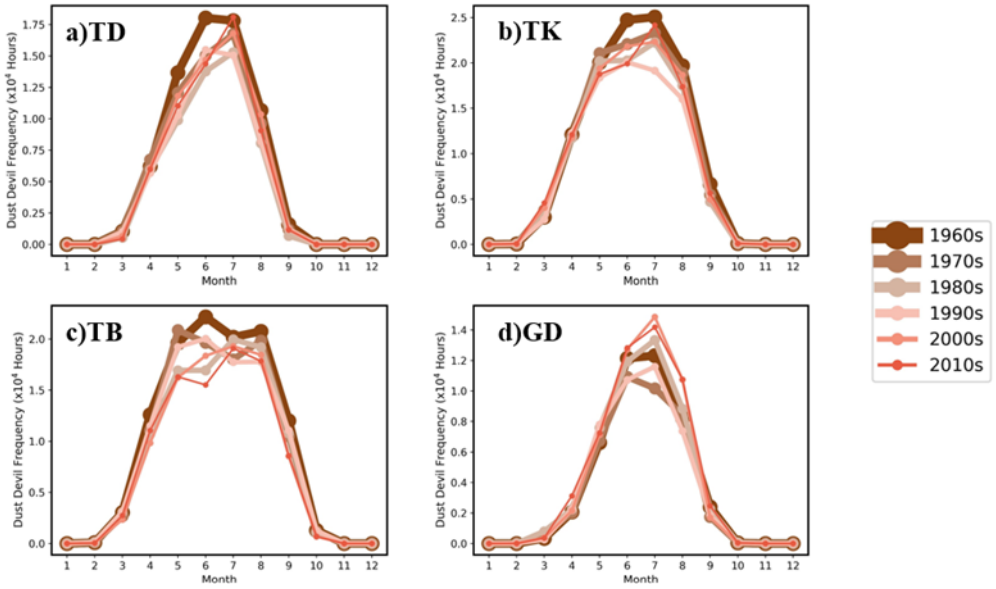

Figure 7. Monthly variation of dust devils at four study sites over the past decades calculated using ERA5 reanalysis dataset.

Figure 7 illustrates the monthly changes of dust devils in six decades at the four study regions. To make the tendency more obvious, the vertical coordinates of the four subplots are not unified. Similar to Figure 5, the frequency of dust devils in different locations started to rise in March and reached its maximum in June and July, with almost no dust devils occurring after September. Unlike Figure 5, in different places, the peak position and the width of the curve varied greatly. The curves of the TD, TK and GD were all single-peak structures, while the TB had a double-peak structure for some decades. The double-peak structure in TB was probably due to uneven distribution of summer precipitation. The average precipitation from May to August was 20.11 mm, 31.17 mm, 37.02 mm and 27.21 mm, respectively, with standard deviation of over 7 mm. In the 2010s, the average precipitation from May to August was 22.11 mm, 43.30 mm, 38.13 mm, 31.65 mm, respectively, where the strong precipitation in June reduced the

frequency of dust devils in June. While in the 1960s, the precipitation in four months was 21.25 mm, 24.77 mm, 33.89 mm and 23.56 mm, respectively, and the high precipitation in July caused the frequency of dust devil to decrease. Full width at half maximum (FWHM) that varies from region to region represents the time of the year when the frequency of dust devil is high, the larger the half-wave width, the longer the dust devil occurrence in a year. In the GD, FWHM occurred between May and August-September, while in the TB, it was between April and September, and for the TD and TK, FWHM was somewhere in between. For the peak shifts, there was a clear trend of peak movement from June to July in the GD and TD, and the peak in the TK area has been mostly in July except in the 1990s, while the peak position has been fluctuating in the TB area due to the influence of precipitation. The effect of volcanic eruptions on the frequency of dust devils is similar to that in Figure 6: Pinatubo eruption caused a significant decrease in the frequency of dust devils in the TD, TK, TB in July 1990s, while the effect on the GD was relatively small. Therefore, the tendency of peak shifts in the 1990s images might be contrary to the overall trend. Ma et al. (2020) presented the single-peaked distribution of monthly changes in dust emissions with a peak in July at the northern margin of the TD, while Han et al. (2016) gave the monthly changes of dust devil frequency in the northwestern China with two peaks in March and June because the dust devil frequency in April was low due to strong winds.

Table 2. Summary of dust devil variation at four study regions over the past decades.

Location Time	TD	TK	TB	GD
1960s	%±16.2%	%±9.0%	%±16.0%	%±7.6%
1970s	% ± 9.0%	%±5.3%	%±10.1%	%±13.0%
1980s	%±6.3%	%±5.0%	%±9.5%	%±12.7%
1990s	%±16.4%	%±4.5%	%±9.4%	%±13.1%
2000s	%±6.9%	%±7.6%	%±6.8%	%±12.2%
2010s	%±7.8%	%±7.1%	%±7.2%	%±10.1%

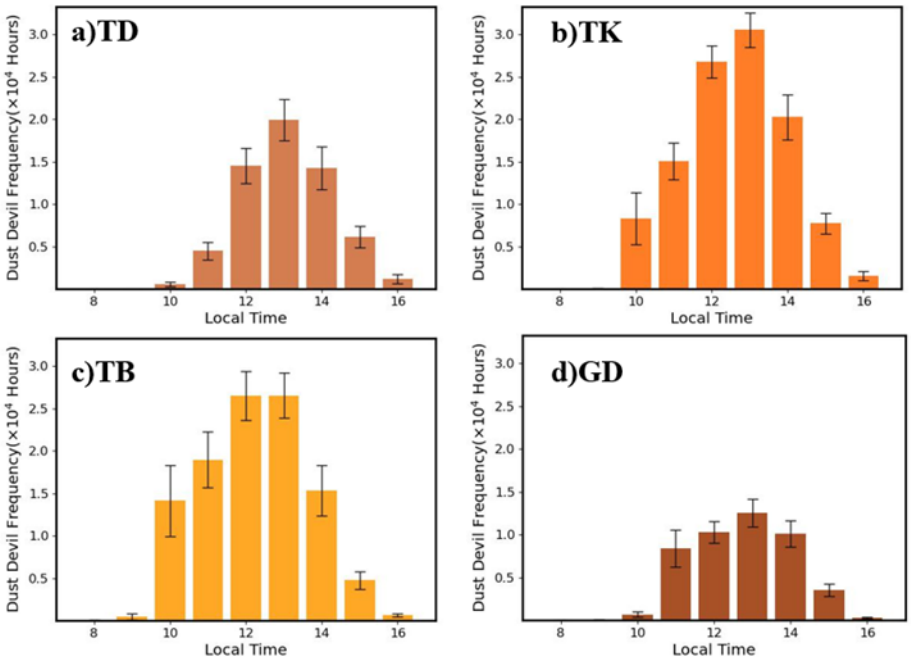

Figure 8. Diurnal variation of dust devils at four study regions in East Asia during 1959-2021 calculated using ERA5 reanalysis dataset.

Changes of dust devils during a day for the four regions calculated based on ERA5 are shown in Figure 8. The black line on the column is the error bar. All times in this chart have been converted to local time in accordance with the time zone divisions. Dust devils primarily occurred in the middle of the day (1000 LT – 1700 LT) with a peak at 1300 LT and started occurring at different times in different regions. In deserts like the TD, GD, dust devil started to increase at 1100 LT while in basin like the TK and TB, the frequency of dust devils was high from 1000 LT onwards. Dust devil frequency between 1200 LT and 1400 LT was more than 60% of the total frequency in the four regions, and for the TD, even reached 80%. Han et al. (2016) presented the diurnal changes in the frequency of dust devil which started at 9000 LT, reached its maximum at 1400 LT, and did not occur after 1700 LT. While Sinclair (1966) found that diurnal changes of dust devil frequency followed a normal distribution with a peak in 1300 LT - 1400 LT. All those previous studies showed a single peaked diurnal changes in dust devil frequency with a peak in 1300LT -1400LT which is quite consistent with our results.

3.3 Relationship between dust devils and meteorological parameters

Under the context of global warming, interannual trends in the frequency of dust devils can vary considerably from region to region. These differences can be attributed to local meteorological factors, e.g., precipitation, air temperature

and wind. This section study how these factors influence dust devil occurrence.

The relationship between precipitation and dust devil frequency is given in Figure 9. Figure 9 contains a total of 252 points for 63 years in the four sites (TD, TK, TB, GD). The color of each point in Figure 9 maps the smoothed spatial density value (kernel density) at which the point is located that the darker the color of the dot, the higher the density of the dot. Anomaly rate on the vertical and horizontal coordinates is the value of that year minus the average of 63 years and divided by the average of 63 years. In this case, precipitation anomaly rate equals the precipitation of that year minus 63 year average divided by the 63 year average precipitation. While on the horizontal coordinate, dust devil frequency anomaly rate is equal to dust devil frequency of that year minus 63 year average divided by 63 year average dust devil frequency. Precipitation data is from ERA5 reanalysis dataset by accumulating hourly data throughout the year while dust devil frequency is calculated using thermodynamic criteria given in section 2.2. The frequency of dust devil and precipitation showed a significant negative correlation at the 99% confidence level. The increase of precipitation will reduce dust devil frequency, and the greater the increase in precipitation, the greater the reduction in dust devils. Liu et al. (2016) reported that rainfall can restrain dust devil frequency by moisturizing the surface even with a large land-air temperature difference, which is consistent with our result. Under the context of global warming, the distribution of precipitation under different scenarios would be very different in 2100 compared to today (IPCC 6, 2021). Therefore, dust devil frequency might change significantly by then.

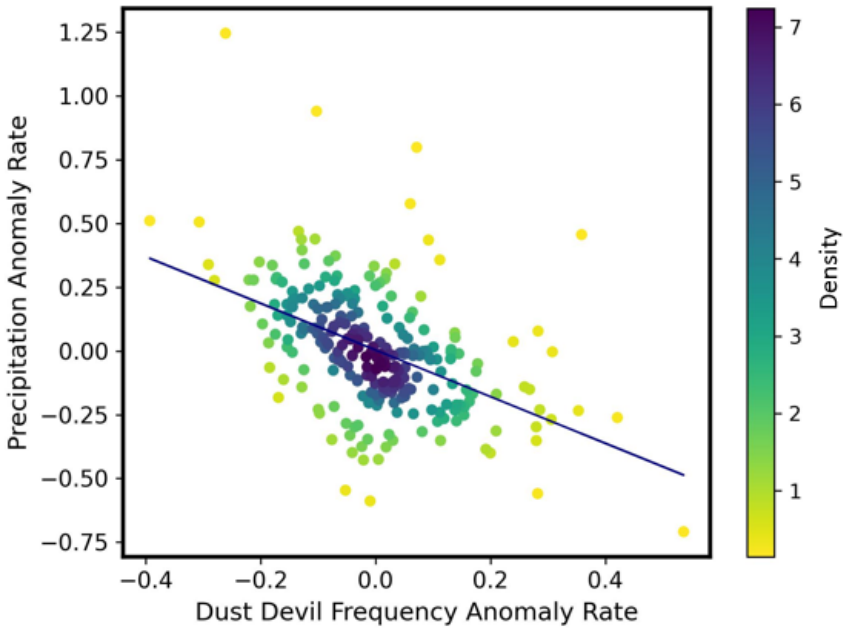

Figure 9. The relationship between precipitation and dust devil frequency in four study regions.

Figure 10 depicts the relationship between air temperature and dust devil frequency. Similar to Figure 9, it contains a total of 252 points for 63 years in four small regions (TD, TK, TB, GD), the darker the color of the dot, the higher the density of the dot. Anomaly rate is defined in the same way as in Figure 9, but the data are for June, July and August, i.e., summer rather than the whole year as the temperature fluctuated greatly during the year and dust devils mostly occurred at midday in summer. In addition, in order to clarify the relationship between the occurrence of dust devil and air temperature, the temperature data were averaged from 1000 LT to 1600 LT in accordance with Figure 9. Air temperature data are from ERA5 reanalysis dataset at 2 m near the ground while dust devil frequency data is also in the corresponding time period. There is a significant positive correlation between air temperature and the frequency of dust devils ($p < 0.01$), and the greater the increase in air temperature, the greater the frequency of dust devils. Compared to Figure 9, the effect of near surface air temperature on dust devils is more diffuse than the effect of precipitation on dust devils. Under global warming, with the rise in temperature, the frequency of dust devils is likely to increase in the future. However, Sinclair (1966) discovered that the highest surface air temperature might not necessarily mean the highest dust devil frequency but the lowest atmospheric (vertical) stability might, implying that the frequency of dust devils could not be determined from the near-surface temperature alone. This is because the frequency of dust devils is influenced by many factors such as precipitation.

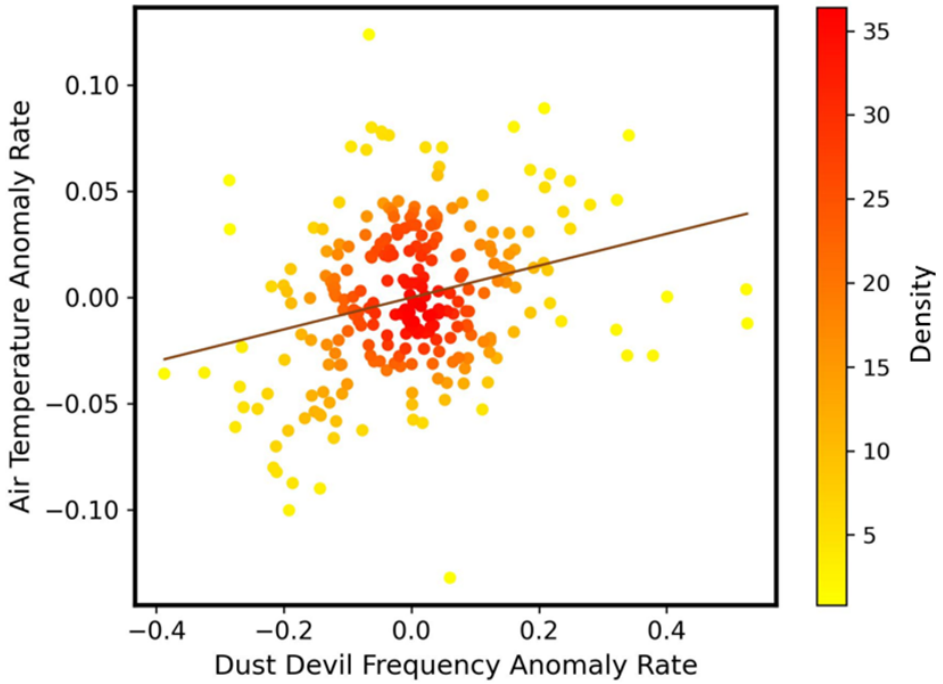

Figure 10. Same as Figure 9 but for air temperature.

The impact of wind speed on the frequency of dust devils is shown in Figure 11. The red bars represent the conditions at the time of the dust devil, while the blue bars represent the time throughout the day. The hourly wind data is from ERA5 reanalysis dataset by the sum of 10m u-component and 10m v-component squared then averaged and only four sites (TD, TK, TB, GD) were counted. Figure 11 shows that the wind speed at the time of dust devil occurrence and throughout the day are both skewed with maximum in 2 m/s and 3m/s, respectively. Dust devils mainly occurred within the interval of wind speed 0-6 m/s. When the wind speed was greater than 8 m/s, dust devils basically ceased to happen. Oke et al. (2007) indicated the occurrence of dust devil at wind speed of around 1.5-7.5 m/s, while Ansmann et al. (2009) mentioned the favorable horizontal wind speed of 2-7 m/s. Han et al. (2016) has confirmed that strong winds are not conducive to the occurrence of dust devils. In that study, they found that dust devil frequency in April was lower than that in March due to frequent strong winds (>17 m/s) in April.

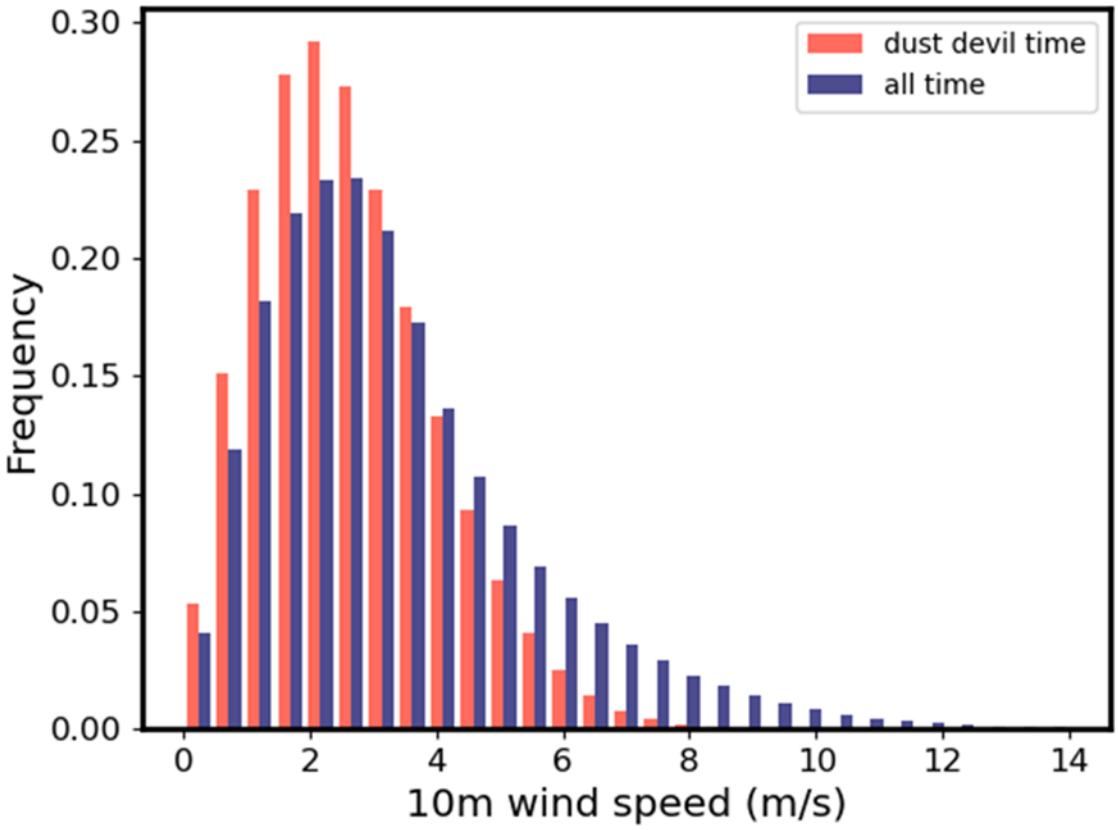

Figure 11. Frequency distribution of wind speed in the duration of dust devils and throughout the day.

4 Conclusions

This paper presented a detailed investigation of long-term variation of dust devils in East Asia, and further analyzed the effect of different underlying surface and meteorological factors on dust devils, mainly based on ERA5 reanalysis dataset. The results show that weak dust devils accounted for about 68% of the total frequency, moderate intensity dust devils occurred about 27%, and strong dust devils happened less than 5% respectively. During 1959-2021, the dust devil frequency in East Asia generally exhibited a downward trend among which strong dust devils dropped significantly declined. Inter-annual trends in dust devil frequency also varied from region to region, with a significant increase of dust devil frequency in the Gobi Desert (GD) but a decrease in the Taklimakan Desert (TD). Moreover, dust devil in East Asia had a distinct seasonal

distribution with the frequency of dust devil reach the highest in summer. In addition, there was a peak for monthly variation of dust devil, shifting from June to July, over the past decades. Regarding the diurnal changes, dust devils mainly occurred between 10:00 LT and 16:00 LT, with over 60% of them occurring between 12:00 LT and 14:00 LT. Particularly, we found a negative correlation between precipitation and dust devil frequency. In addition, dust devils mainly occurred at wind speed of 0–6 m/s and almost no dust devil happened when the 10-m wind speed is larger than 8 m/s. This study provides a comprehensive understanding of dust devils in East Asia over the past decades, which is of great importance to further evaluate its impact on climate, environment as well as ecosystem.

Acknowledgments

This research was funded by the Second Tibetan Plateau Scientific Expedition and Research Program (STEP), Grant No. 2019QZKK0602, National Natural Science Foundation of China (41875029); Higher Education Discipline Innovation Project – 111 Project (B 13045).

Open Research

Data Availability Statement

The ERA5 reanalysis dataset are available at https://www.ecmwf.int/en/forecasts/dataset/ecmwf-reanalysis-v5 and can be downloaded using Climate Data Store (CDS). Calculations and plotting have largely been performed using the Python software (Python Software Foundation, https://www.python.org/).

References

Ansmann, A., Tesche, M., Knippertz, P., Bierwirth, E. & Schulz, O. (2009). Vertical profiling of convective dust plumes in southern morocco during samum. *Tellus B*, 61(1).

Balme, M., & Greeley, R. (2006). Dust devils on earth and mars. *Reviews of Geophysics*, 44(3).

Burrows, S. M., Elbert, W., Lawrence, M. G., & Pöschl, U. (2009). Bacteria in the global atmosphere–Part 1: Review and synthesis of literature data for different ecosystems. Atmospheric Chemistry and Physics, 9(23), 9263-9280.

Carroll, J. J., & Ryan, J. A. (1970). Atmospheric vorticity and dust devil rotation. *Journal of Geophysical Research*, 75(27), 5179-5184.

Copernicus Climate Change Service (C3S) (2017). ERA5: Fifth generation of ECMWF atmospheric reanalyses of the global climate. Copernicus Climate Change Service Climate Data Store (CDS).

Deardorff, J. W. (1970), Convective velocity and temperature scales for the unstable planetary boundary layer and for Rayleigh convection, *J. Atmos. Sci.*, 27, 1211–1213.

Dee, D. P., Uppala, S. M., Simmons, A. J., Berrisford, P., Poli, P., Kobayashi, S., et al. (2011). The ERA-Interim reanalysis: Configuration and performance of the data assimilation system. *Quarterly Journal of the Royal Meteorological Society*, 137, 553– 597.

Després, Viviane R., Alex Huffman, J., Burrows, S. M., Hoose, C., Safatov, A. S., & Buryak, G., et al. (2012). Primary biological aerosol particles in the atmosphere: a review. *Tellus Series B-chemical & Physical Meteorology*, 64.

Dong, Q., Huang, Z., Li, W., Li, Z., Song, X., Liu, W., ... and Shi, J. (2022). Polarization Lidar Measurements of Dust Optical Properties at the Junction of the Taklimakan Desert–Tibetan Plateau. *Remote Sensing*, *14*(3), 558.

Douwes, J., Thorne, P., Pearce, N., & Heederik, D. (2003). Bioaerosol health effects and exposure assessment: progress and prospects. *The Annals of occupational hygiene*, 47(3), 187-200.

FAO (Food and Agriculture Organization of the United Nations). (1977). World Map of Desertification. Food and Agricultural Organization (FAO), Rome.

Feng, S., & Fu, Q. (2013). Expansion of global drylands under a warming climate. *Atmospheric Chemistry and Physics*, 13(10), 081-094. Doi:10.5194/acp-13-10081-2013.

Gao, C., Xiu, A., Zhang, X., Tong, Q., Zhao, H., Zhang, S., Yang, G., and Zhang, M.: Two-way coupled meteorology and air quality models in Asia: a systematic review and meta-analysis of impacts of aerosol feedbacks on meteorology and air quality, *Atmos. Chem. Phys.*, 22, 5265–5329, https://doi.org/10.5194/acp-22-5265-2022, 2022.

Gillette, D. A. and Sinclair, P. C. Estimation of suspension of alkaline material by dust devils in the United States (1990). *Atmos. Environ.*, 24, 1135–1142.

Ginoux, P., M., Chin, I., Tegen, M., Prospero, B., Holben, O., Dubovic, and S. J., Lin (2001), Sources and distributions of dust aerosols simulated with the GOCART model, *J. Geophys. Res.*, 106, 20255–20273.

Gu, Z. L., Qiu, J., Zhao, Y. Z., & Hou, X. P. (2008). Analysis on dust devil containing loess dusts of different sizes. *Aerosol & Air Quality Research*, 8(1), 65-77.

Gu, Z. L., Wei, W., & Zhao, Y. Z. (2010). An overview of surface conditions in numerical simulations of dust devils and the consequent near-surface air flow fields. *Aerosol and Air Quality Research*, 10(3), 272-281.

Han, Y., Wang, K., Liu, F., Zhao, T., Yin, Y., Duan, J., Luan, Z. (2016). The contribution of dust devils and dusty plumes to the aerosol budget in western China. *Atmos. Environ.* 126, 21–27.

Hersbach, H., Bell, B., Berrisford, P., Biavati, G., Horányi, A., Muñoz Sabater, J., Nicolas, J., Peubey, C., Radu, R., Rozum, I., Schepers, D., Simmons, A., Soci, C., Dee, D., Thépaut, J-N. (2018): ERA5 hourly data on single levels

from 1959 to present. Copernicus Climate Change Service (C3S) Climate Data Store (CDS). (Accessed on 14-APR-2021), 10.24381/cds.adbb2d47

Hess, G.D. and Spillane, K.T. Characteristics of Dust Devils in Australia. *J. Appl. Meteorol.* 1990, 29: 498– 507.

Hoose, C., & Möhler, O. (2012). Heterogeneous ice nucleation on atmospheric aerosols: a review of results from laboratory experiments. *Atmospheric Chemistry and Physics*, 12(20), 9817-9854.

Huang, J., Yu, H., Dai, A. *et al.* Drylands face potential threat under 2 °C global warming target. *Nature Clim Change* **7,** 417–422 (2017). https://doi.org/10.1038/nclimate3275

Huang, J., Zhang, G., Zhang, Y., Guan, X., Wei, Y., & Guo, R. (2020). Global desertification vulnerability to climate change and human activities. *Land Degradation & Development*, 31(11), 1380-1391.

Huang, Z., Huang, J., Bi, J., Wang, G., Wang, W., Fu, Q., ... & Shi, J. (2010). Dust aerosol vertical structure measurements using three MPL lidars during 2008 China-US joint dust field experiment. *Journal of Geophysical Research: Atmospheres*, *115*(D7).

Huang, Z., Nee, J. B., Chiang, C. W., Zhang, S., Jin, H., Wang, W., & Zhou, T. (2018). Real-Time Observations of Dust–Cloud Interactions Based on Polarization and Raman Lidar Measurements. *Remote Sensing*, *10*(7), 1017.

Huang, Z., Wang, Y., Bi, J., Wang, T., Li, W., Li, Z., & Zhou, T. (2022). *An overview of aerosol lidar: progress and prospect*, 26(5), 834–851. doi: 10.11834/jrs.20221388.

IPCC, 2021: Climate Change 2021: The Physical Science Basis. Contribution of Working Group I to the Sixth Assessment Report of the Intergovernmental Panel on Climate Change[Masson-Delmotte, V., P. Zhai, A. Pirani, S.L. Connors, C. Péan, S. Berger, N. Caud, Y. Chen, L. Goldfarb, M.I. Gomis, M. Huang, K. Leitzell, E. Lonnoy, J.B.R. Matthews, T.K. Maycock, T. Waterfield, O. Yelekçi, R. Yu, and B. Zhou (eds.)]. *Cambridge University Press*, Cambridge, United Kingdom and New York, NY, USA, In press, doi:10.1017/9781009157896.

Jemmett-smith, B., Marsham, J., Knippertz, P. & Gilkeson, C. (2015). Quantifying global dust devil occurrence from meteorological analyses. *Geophysical Research Letters*, 42(4), 1275-1282.

Klose, M. R. (2014). Convective Turbulent Dust Emission: Process, parameterization, and relevance in the Earth system (Doctoral dissertation, Universität zu Köln).

Klose, M., Jemmett-Smith, B. C., Kahanp, H., Kahre, M., Knippertz, P., & Lemmon, M. T., et al. (2016). Dust devil sediment transport: from lab to field to global impact. *Space Science Reviews*, 1-50.

Koch, J. & Renno, N. O. (2005). The role of convective plumes and vortices on the global aerosol budget. *Geophysical Research Letters*, 32(18).

Kok, J. F., Adebiyi, A. A., Albani, S., Balkanski, Y., & Wan, J. S. (2021). Contribution of the world's main dust source regions to the global cycle of desert dust. *Atmospheric Chemistry and Physics*, 21(10), 8169-8193.

Klose, M., & Shao, Y. (2016). A numerical study on dust devils with implications to global dust budget estimates. *Aeolian Research*, 22, 47-58.

Liu, C., Zhao, T., Yang, X., Liu, F., Han, Y., & Luan, Z. et al. (2016). Observational study of formation mechanism, vertical structure, and dust emission of dust devils over the Taklimakan desert, China. J*ournal of Geophysical Research Atmospheres*, 121(7).

Liu, J., Xin, Z., Huang Y., Yu J. (2022). Climate suitability assessment on the Qinghai-Tibet Plateau, *Science of The Total Environment,* Volume 816, 151653.

Liu, Q., Huang, Z., Hu, Z., Dong, Q., & Li, S. (2022). Long-range transport and evolution of Saharan dust over East Asia from 2007 to 2020. *Journal of Geophysical Research: Atmospheres*, e2022JD036974.

Lyons, T. J., U. S. Nair, and I. J. Foster (2008), Clearing enhances dust devil formation, *J. Arid Environ.*, 72, 1918–1928.

Maki, T., Kakikawa, M., Kobayashi, F., Yamada, M., Matsuki, A., & Hasegawa, H., et al. (2013). Assessment of composition and origin of airborne bacteria in the free troposphere over japan. *Atmospheric Environment*, 74, 73-82.

Maki, T., Puspitasari, F., Hara, K., Yamada, M., Kobayashi, F., Hasegawa, H., & Iwasaka, Y. (2014). Variations in the structure of airborne bacterial communities in a downwind area during an Asian dust (Kosa) event. *Science of the total environment*, 488, 75-84.

Ma, M., Yang, X., Zhou, C., He, Q. & Mamtimin, A. (2020). Contributions of dusty weather and dust devil to dust emission amounts at the northern margin of the Taklimakan desert. *Natural Hazards*, 103(1).

Mason, J. P., Patel, M. R. & Lewis, S. R. (2014). The retrieval of optical properties from terrestrial dust devil vortices. *Icarus*, 231(4), 385-393.

Metzger S.M., Balme M.R., Towner M.C., Bos, B.J., Ringrose T.J., Patel M.R. (2011) In situ measurements of particle load and transport in dust devils. *Icarus*, 214(2), 766–772.

Morris, C. E., Conen, F., Huffman, J. A., Phillips, V., Ulrich Pöschl, & Sands, D. C. (2014). Bioprecipitation: a feedback cycle linking earth history, ecosystem dynamics and land use through biological ice nucleators in the atmosphere. *Global Change Biology*, 20(2).

Neakrase L.D.V., Greeley R. (2010). Dust devil sediment flux on Earth and Mars: laboratory simulations. *Icarus* 206(1), 306–318.

Oke, A., Tapper, N. J. & Dunkerley, D. (2007). Willy-willies in the australian landscape: the role of key meteorological variables and surface conditions in defining frequency and spatial characteristics. *Journal of Arid Environments*, 71(2), 201-215.

Pöschl, U., Martin, S. T., Sinha, B., Chen, Q., Gunthe, S. S., Huffman, J. A., ... & Andreae, M. O. (2010). Rainforest aerosols as biogenic nuclei of clouds and precipitation in the Amazon. *science*, 329(5998), 1513-1516.

Pöschl, U., & Shiraiwa, M. (2015). Multiphase chemistry at the atmosphere–biosphere interface influencing climate and public health in the anthropocene. *Chemical Reviews*, 115(10), 4440-4475.

Renno, N. O., et al. (2004), MATADOR 2002: A pilot field experiment on convective plumes and dust devils, *J. Geophys. Res.*, 109, E07001.

Ryan, J. A. (1972), Relation of dust devil frequency and diameter to atmospheric temperature, *Geophys. Res. Lett.*, 77, 7133–7137.

Sesartic, A., Lohmann, U., & Storelvmo, T. (2012). Bacteria in the echam5-ham global climate model. Atmospheric Chemistry and Physics, 12(18), 8645-8661.

Self, S., Zhao, J.-X., Holasek, R. E., Torres, R. C., and King, A.J. (1996) The atmospheric impact of the 1991 Mount Pinatubo erup-tion, in: Fire and Mud: Eruptions and lahars of Mount Pinatubo,Philippines, *University of Washington Press*.

Shao Y., Wyrwoll K., Chappell A., Huang J., Lin Z. et al. (2011). Dust cycle: an emerging core theme in earth system science. *Aeolian Research*, 2(4), 181-204.

Sinclair, P. C. (1966), A quantitative analysis of the dust devil, Ph.D. thesis, Univ. of Ariz., Tucson.

Sinclair, P. C. (1973). The lower structure of dust devils. *Journal of the Atmospheric Sciences*, 30(8), 1599-1619.

Tanarhte, M., Bacer, S., Burrows, S. M., Huffman, J. A., Pierce, K. M., Pozzer, A., ... & Lelieveld, J. (2018). Global modeling of primary biological particle concentrations with the EMAC chemistry-climate model. *Atmospheric Chemistry and Physics Discussions*, 1-33.

Tang, K., Huang, Z., Huang, J., Maki, T., Zhang, S., Shimizu, A., Ma, X., Shi, J., Bi, J., Zhou, T., Wang, G., & Zhang, L. (2018). Characterization of atmospheric bioaerosols along the transport pathway of Asian dust during the Dust-Bioaerosol 2016 Campaign. A*tmospheric Chemistry and Physics*, 18(10), 7131-7148.

Tegen, I., Harrison, S.P., Kohfeld, K., Prentice, I.C., Coe, M., Heimann, M., (2002). Impact of vegetation and preferential source areas on global dust aerosol: Results from a model study. *J. Geophys. Res.* 107, 4576.

Wang, J., Guan, X., Guan, Y., Zhu, K., Shi, R., Kong, X., & Guo, S. (2021). Changes in lengths of the four seasons over the drylands in the northern hemisphere midlatitudes. *Journal of Climate*, *34*(20), 8181-8190.

Xu, X., Wang, X., & Huang, J. (2011). Observational study on the particle size distribution of sand aerosol in Zhangye and Yuzhong of Lanzhou. Plateau Meteorol, 30, 208-216.

Zhang, S., Huang, Z., Li, M., Shen, X., Wang, Y., Dong, Q., ... & Song, X. (2022). Vertical Structure of Dust Aerosols Observed by a Ground-Based Raman Lidar with Polarization Capabilities in the Center of the Taklimakan Desert. Remote Sensing, 14(10), 2461.

Zhao, Y. Z., Gu, Z. L., Yu, Y. Z., Ge, Y., Li, Y. & Feng, X. (2004) Mechanism and large eddy simulation of dust devils, *Atmosphere-Ocean*, 42:1, 61-84.